EARTHQUAKE ENGINEERING AND STRUCTURAL DYNAMICS
Earthquake Engng Struct. Dyn. 2008; **37**:627–645
Published online 19 December 2007 in Wiley InterScience (www.interscience.wiley.com). DOI: 10.1002/eqe.779

Seismic self-centering steel beam-to-column moment connections using bolted friction devices

Keh-Chyuan Tsai[1, 2, *, †, ‡, §], Chung-Che Chou[3, ¶], Chi-Lon Lin[1, ‖], Pei-Ching Chen[2, **] and Sheng-Jhih Jhang[2, **]

[1]*Department of Civil Engineering, National Taiwan University, Taipei, Taiwan*
[2]*National Center for Research on Earthquake Engineering, Taipei, Taiwan*
[3]*Department of Civil Engineering, National Chiao Tung University, Hsinchu, Taiwan*

SUMMARY

This paper first presents the force–deformation relationship of a post-tensioned (PT) steel beam-to-column connection constructed with bolted web friction devices (FDs). This paper then describes the test program conducted in the National Center for Research on Earthquake Engineering, Taiwan, on four bolted FDs and four full-scale PT beam-to-column moment connection subassemblies using the FDs. Tests confirm that (1) the hysteretic behavior of four bolted FDs is very stable, (2) the friction coefficient between the steel plate and the brass shim is about 0.34, (3) the proposed force–deformation relationships reasonably predict the experimental responses of the PT connections under cyclically increasing deformations up to a beam peak rotation of 0.05 rad, and (4) the decompression moments do not degrade as beam cyclic deformations increase. Copyright © 2007 John Wiley & Sons, Ltd.

Received 1 November 2006; Revised 29 October 2007; Accepted 30 October 2007

KEY WORDS: post-tensioned connection; self-centering; friction device

1. INTRODUCTION

The connection with steel beams post-tensioned (PT) to a steel column is self-centering without residual deformation. The connection eliminates the use of field groove welding at the beam-to-column interface and also buckling of the beam in cyclic tests. Because there is no

*Correspondence to: Keh-Chyuan Tsai, Department of Civil Engineering, National Taiwan University, Taipei, Taiwan.
†E-mail: kctsai@ncree.org.tw
‡Professor.
§Director.
¶Associate Professor.
‖Graduate Research Assistant.
**Assistant Research Fellow.

Contract/grant sponsor: National Science Council of Taiwan

energy dissipation for the connection with only a column and PT beams, various kinds of energy dissipation devices such as seat angles, round bars, or reduced flange plates have been used to increase the energy dissipation of the connection [1–5]. Cyclic tests have also been undertaken on full-scale interior PT beam-to-column connections subjected to either fatigue loading or twice the AISC standard loading [6] to investigate the energy dissipation capacity and durability of the round bars [7]. After many cyclic tests, it was difficult to replace these damaged devices due to interference with the composite slab or welded joints between the beam and the devices.

Cyclic tests of PT connections using friction energy dissipation devices, which are placed only below the beam bottom flange, have demonstrated excellent energy dissipation without failure of the devices and without residual drift [8, 9]. This study [10] contributes further insight into the seismic performance of PT steel connections using the bolted web friction device (BWFD). An analytical model is first presented and the cyclic uni-axial tests conducted on four BWFDs are then examined. Four exterior beam-to-column connections, each of which includes an $H350\times 350\times 12\times 19$ wide flange column, an $H500\times 200\times 10\times 16$ beam, and a BWFD, are also tested in the National Center for Research on Earthquake Engineering (NCREE) in Taiwan. The study has the following objectives: (1) to develop a hysteretic model for the PT connection with a BWFD, (2) to investigate the friction response of the BWFD containing a brass plate between two steel plates, and (3) to examine the cyclic performance of the PT connections, with a BWFD, subjected to multiple AISC standard loadings [6]. The parameters in these tests include the initial PT force, the washer type, and the number and size of high-strength bolts used to connect the beam web and the friction energy dissipation device. This paper presents experimental and analytical results of these PT connections and friction energy dissipation devices subjected to cyclic inelastic loading.

2. ANALYTICAL MODELS FOR PT STEEL BEAM-TO-COLUMN MOMENT CONNECTIONS USING WEB FRICTION DEVICES

A PT steel beam-to-column moment connection using web friction devices (FDs) is shown in Figure 1. Two wide flange beams are connected to a wide flange column through two beam web FDs. Each FD consists of two web clamping plates welded to the column flange and connected to the beam web using slip-critical bolts. PT tendons run along two sides of the beam web and run through the column flanges. Properly proportioned PT tendons should ensure a bi-linear elastic response of the PT beam-to-column connection while the web FD dissipates stable energy. Thus, a properly designed PT beam-to-column connection with FD (PTFD) should possess desirable re-centering and sufficient energy dissipation capabilities.

2.1. Hysteretic behavior of a PTFD connection

Figure 2 shows the free body diagram of a typical PTFD connection. Point A in the flag-shape hysteresis loop shown in Figure 3 is called the 'decompression point'. At this point, the gap at the beam-to-column interface is at the onset of opening. Before reaching the decompression point, the behavior of the PTFD connection is very similar to the elastic response of a conventional welded moment connection [1]. However, after the decompression moment, M_A, is exceeded, a gap opens and the beam end near the column flange rotates. The center of rotation is near the junction between the beam flange and beam web [1–4]. The relative displacement between the

DOI: 10.1002/eqe

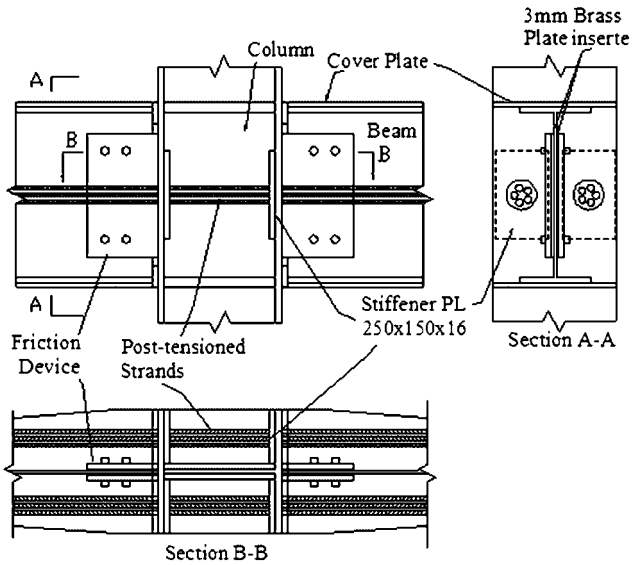

Figure 1. Schematic of post-tensioned beam-to-column connection using friction devices.

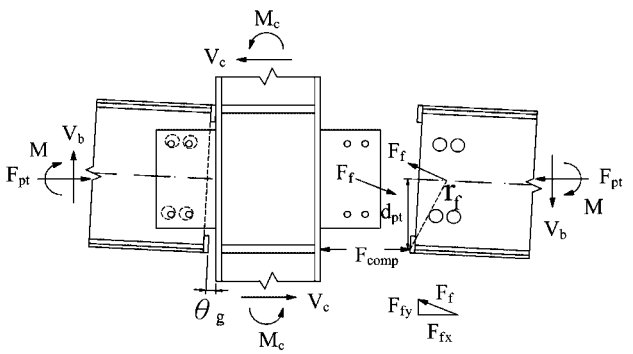

Figure 2. Free body diagram of a PTFD connection at the beam-to-column interface.

clamping plates and the beam web activates the FD, introducing energy dissipation. If the load is reversed at point B, the friction force develops after point C.

The total compression force F_{comp} (Figure 2) is equal to the PT force plus the friction force provided by the FD, and is expressed as

$$F_{\text{comp}} = F_{\text{pt},i} + \Delta F_{\text{pt}} + F_{\text{f}x} \tag{1}$$

where $F_{\text{f}x}$ is the horizontal component of the friction force F_{f}, $F_{\text{pt},i}$ is the initial PT force, and ΔF_{pt} is the PT force increment due to the gap opening at the beam-to-column interface. The PT

DOI: 10.1002/eqe

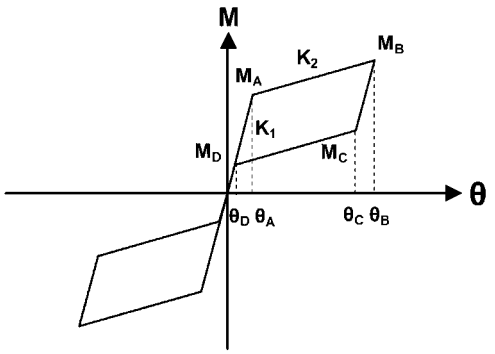

Figure 3. PTFD beam moment *versus* rotation relationship.

force increment ΔF_{pt} is a function of θ_g [4]:

$$\Delta F_{\mathrm{pt}} = \frac{2EA_{\mathrm{pt}}d_{\mathrm{pt}}\theta_g}{L_{\mathrm{pt}}}\left(1-\frac{A_{\mathrm{pt}}}{A_{\mathrm{b}}+A_{\mathrm{pt}}}\right) \tag{2}$$

where E is the elastic modulus of the tendon, A_{pt} is the cross-sectional area of all tendons, and A_{b} is the cross-sectional area of the beam, L_{pt} is the tendon length, and d_{pt} is the distance from the center of PT force to the center of rotation.

Assuming that the friction coefficient is constant over the friction surface, the friction force F_{f} is

$$F_{\mathrm{f}} = \mu n_{\mathrm{b}} F_{\mathrm{b}} n_{\mathrm{fs}} \tag{3}$$

where μ is the friction coefficient, n_{b} is the number of bolts, F_{b} is the pretension force in each bolt, and n_{fs} is the number of friction surfaces. The beam moment is calculated as

$$\begin{aligned} M &= M_{\mathrm{pt}} + M_{\mathrm{f}} \\ &= (F_{\mathrm{pt},i} + \Delta F_{\mathrm{pt}})d_{\mathrm{pt}} + F_{\mathrm{f}} r_{\mathrm{f}} \end{aligned} \tag{4}$$

where r_{f} is the distance from the center of rotation to the centroid of the friction force, M_{pt} and M_{f} are the beam moments provided by the PT force and the BWFD, respectively. The PT force is constant before the gap opening; hence, the decompression moment M_A at point A (Figure 3) is equal to

$$\begin{aligned} M_A &= M_{\mathrm{pt},i} + M_{\mathrm{f}} \\ &= F_{\mathrm{pt},i} d_{\mathrm{pt}} + F_{\mathrm{f}} r_{\mathrm{f}} \end{aligned} \tag{5}$$

Figure 3 shows the beam moment and rotation relationship; the rotation is calculated as the beam displacement divided by the length measured from the applied load to the column centerline. The flexural stiffness of a PT connection subassembly is provided by the column, beam, panel zone, and PT tendons. The elastic flexural stiffness K_1 of the PT connection subassembly is similar to that of a typical welded moment connection subassembly before the gap opening [1]. The behavior of the connection, then, becomes nonlinear. The stiffness of the web FD becomes zero upon decompression, and the flexural stiffness of the subassembly is associated with that of

DOI: 10.1002/eqe

the column, beam, panel zone, and PT tendons. The flexural stiffness K_2 of the PT connection subassembly is equal to

$$K_2 = \frac{1}{1/K_c + 1/K_b + 1/K_{pz} + 1/K_{pt}} \tag{6}$$

where K_c, K_b, K_{pz}, K_{pt} are the flexural stiffness provided by the steel column, beam, panel zone, and PT tendons, respectively. Since the steel column, beam, and panel zone remain elastic throughout the test, the flexural stiffnesses of these components can be found elsewhere [11]. The beam moment increment provided by the PT tendons is calculated based on the PT force increment [Equation (2)] times the distance d_{pt} [4]. Assuming a rigid body rotation of the beam about the compression toe, the flexural stiffness K_{pt} can be determined as

$$K_{pt} = \frac{2EA_{pt}d_{pt}^2(L_b + d_c/2)}{L_{pt}L_b}\left(1 - \frac{A_{pt}}{A_b + A_{pt}}\right) \tag{7}$$

where L_b is the length of the beam measured from the column face, and d_c is the depth of the column.

When the applied moment reaches the decompression moment M_A, the beam rotation θ_A is computed as the decompression moment M_A divided by the flexural stiffness K_1. With the increase of the load, the beam moment M_B at the maximum deformation is equal to

$$M_B = M_A + K_2(\theta_B - \theta_A) \tag{8}$$

Upon unloading to point C, the beam moment and rotation are

$$M_C = M_B - 2M_f \tag{9}$$

$$\theta_C = \theta_B - \frac{2M_f}{K_1} \tag{10}$$

where M_f is obtained from Equation (4). As the applied moment continues to decrease, the gap opening decreases. The beam moment and rotation at point D are equal to

$$M_D = M_A - 2M_f \tag{11}$$

$$\theta_D = \theta_C - \frac{M_C - M_D}{K_2} \tag{12}$$

Both the beam moment and gap rotation, then, return to zero; hence, the connection subassembly re-centers. A symmetric response is obtained when the load is applied in the opposite direction.

3. EXPERIMENTAL TESTING OF INDIVIDUAL FDs

FDs have been studied quite extensively in the past [8, 9, 12, 13]. Rojas *et al.* [8] investigated the cyclic performance of PT connections using friction joints at the beam top and bottom flanges. Wolski *et al.* [9] studied the cyclic performance of PT connections using an FD installed only under the beam bottom flange. The beam bottom flange FD adopted inclined slotted holes. Grigorian and Popov [12] investigated the cyclic response of slotted FDs for steel braced frames, and concluded

DOI: 10.1002/eqe

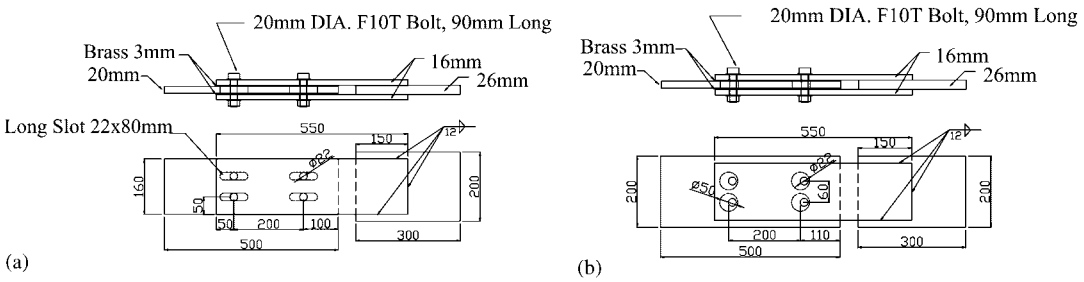

Figure 4. Details of bolted friction device specimens: (a) Specimens SF and SB and (b) Specimens CF and CB.

that Belleville washers and the brass shims adopted in the slotted joint could provide stable friction forces. Morgen and Kurama [13] performed studies to investigate the performance of precast concrete moment connections with friction. Oversized circular holes were never adopted in these previous studies. Thus, effects of slotted *versus* circular holes, as well as flat *versus* Belleville washers, on the cyclic performance of the connections were investigated in this study.

A total of four FD specimens (SF, SB, CB, and CF) as shown in Figure 4 were tested. A C1202 grade 3 mm thick brass shim plate was placed between all the interfaces where friction was to be developed. The first character (S or C) of the Specimen ID stands for the shape (slotted or circular) of the oversized bolt holes. The second character (F or B) of the Specimen ID identifies the type (flat or Belleville) of washers adopted in the FD specimens. Each specimen was constructed by clamping two 16 mm thick steel outer plates over one 20 mm thick center plate. All steel plates are of a A572 GR50 steel. In each specimen, four F10T 20 mm diameter bolts were adopted, and the oversized holes were made only on the 20 mm thick center plates. F10T high-tension bolts are commonly adopted in the connections of steel structures, and the method of achieving pre-load follows the AISC specifications [14]. Therefore, there is no consideration on the long-term relaxation of bolt pre-load. The size of the slotted holes is 22×80 mm and the diameter of the oversized circular holes is 50 mm. For specimens with slotted holes, Specimen SF was tested first, and then the bolts and the flat washers were removed before installing new bolts and Belleville washers for the testing of Specimen SB. For specimens with circular oversized holes, Specimen CB was tested first before installing new bolts and the flat washers for the testing of Specimen CF. Before installing the bolts, the bolts were instrumented and calibrated so that a specific pre-load (150 kN for Specimens SF, SB, 180 kN for Specimens CB and CF) in each bolt was ensured. Each FD specimen with slotted holes was tested in a uni-axial universal testing machine through a series of symmetrical displacement cycles. The displacement history consisted of six cycles with displacement amplitudes of 5, 10, 20, and 30 mm. However, specimens with circular holes were loaded in only one direction to the pre-described displacement amplitude. The loading rate was 2 mm/s for all specimen tests.

3.1. Cyclic responses of bolted FDs

3.1.1. Specimen SF. Figure 5(a) gives the complete 42 cyclic force *versus* displacement relationships. Figure 5(b) shows the first 24 cycles of responses, while Figure 5(c) gives the results of the last 18 cycles. Vibration and noise induced by friction were rather pronounced in the beginning of

DOI: 10.1002/eqe

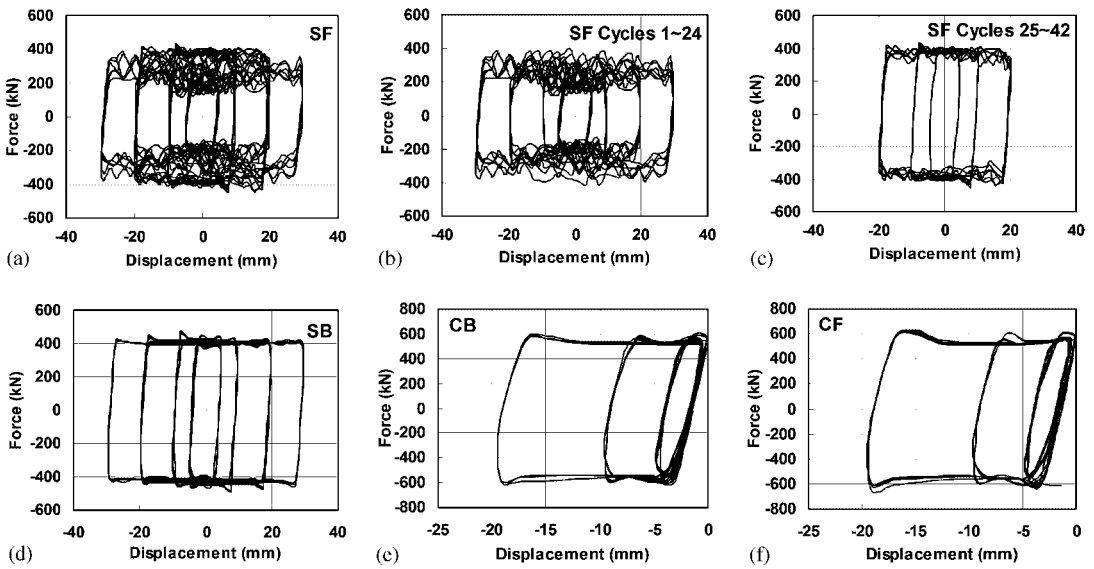

Figure 5. Force *versus* displacement relationships of friction device specimens: (a) Specimen SF; (b) the first 24 cycles of response of Specimen SF; (c) the 25–42 cycles of response of Specimen SF; (d) Specimen SB; (e) Specimen CB; and (f) Specimen CF.

the test, as evidenced by the jagged edges of the hysteresis loops (Figures 5(a) and (b)). However, after the peak displacement (30 mm) was developed in the first 24 cycles, the friction interfaces seemed to have been sufficiently worn, leading to reduced vibration and noise as illustrated by comparing Figures 5(b) and (c). Furthermore, Figure 5(c) shows a marked increase in the friction force for cycles 25–42. However, when the Belleville washers were adopted, the cyclic responses were much more stable throughout the tests. This seems to suggest that the temperature in the brass shim plates could have been substantially increased and the expansion of the shims increased the bolt clamping forces as evidenced in the increase of the bolt strains.

3.1.2. Specimen SB. After the new bolts and Belleville washers were installed, Figure 5(d) shows a further smoothed force *versus* displacement relationships when compared with Figure 5(c).

3.1.3. Specimen CB. Specimen CB was tested before Specimen CF to investigate the effects of the Belleville washers on a new friction interface. The pre-load of the bolts was increased to 180 kN for Specimens CB and CF. In order to simulate a realistic situation for the FD installed in PTFD connections, cyclically increasing displacements are not symmetric with respect to the initial un-deformed position. Figure 5(e) shows smoothed force *versus* displacement relationships when compared with Figure 5(b). Vibration and noise due to friction were greatly reduced in the very beginning of the test.

3.1.4. Specimen CF. Figure 5(f) also shows smoothed force *versus* displacement relationships when compared with Figure 5(c), indicating that vibration and noise due to friction were not

DOI: 10.1002/eqe

evident. Based on these tests, the following conclusions can be drawn:

(1) Vibration and noise due to friction are pronounced without using Belleville washers when the friction surface is new. In addition, friction forces tend to increase as cyclic displacements increase.
(2) When the friction surface has been worn, an almost constant friction force can be achieved.
(3) For larger bolt pre-loads, greater friction noise and vibration are likely to occur for the same friction interface. Comparing Figures 5(e) and (b), it is evident that the Belleville washers effectively reduced the friction noise and vibration.
(4) Comparing the responses of Specimen SB (four bolts each pre-loaded to 150 kN) and specimen CB (four bolts each pre-loaded to 180 kN), it can be found that the friction coefficient is about the same (0.34 *versus* 0.37). This suggests that the effects of the oversized hole pattern (slotted or circular) on the magnitude of the friction coefficient are not significant.

4. EXPERIMENTAL TESTING OF FULL-SCALE PTFD CONNECTIONS

Four specimens using BWFDs (4B20S, 4B20, 6B20, and 4F22) were designed, fabricated, and tested at the NCREE to investigate the seismic performance of the PTFD connections. Each specimen represented a typical exterior beam-to-column connection subassembly with one beam attached to one column. Since the column section was expected to remain elastic throughout the tests, two beams each with its own FD were simultaneously connected to the same column. Brass was adopted to provide stable contact surface between steel plates and was not replaced after each test to investigate the performance of these devices subjected to multiple cyclic loads.

4.1. Design of specimens

Figure 6 shows details of four PT connections using BWFDs. All beam sections were identical ($H500\times200\times10\times16$ mm), and cover plates were added to the beam flanges to ensure that the beam remained elastic. The trapezoidal-shape cover plates were 16 mm thick, 1100 mm long, 350 and 220 mm wide. One column section ($H350\times350\times12\times19$ mm) was fabricated and repeatedly used in this study. The column size was determined based on strong-column weak-beam principles. All steel was A572 GR50. A total of four 100-mm diameter holes were drilled in the column flanges (Figure 1) for passing tendons; hence, four stiffeners each measuring 250 by 150- and 16-mm thick were welded on to the inner faces of the column flanges for retrofitting. Two 16 mm thick doubler plates were installed in the beam-to-column panel zone joint. All the column continuity plates were 28 mm thick. The size of the oversized circular bolt holes on the beam web was determined from the requirement of a maximum beam rotation of 0.05 rad. In order to ensure the re-centering mechanism, the lower bound of the initial PT tendon force is determined from the peak friction force. However, the upper bound of the initial PT force is determined based on a number of factors, including the beam peak rotational demand, the maximum allowed tendon stress, and the combined axial–flexural capacity of the beam. The ratios of the flexural strength between the PT beam and the energy dissipation device that have been identified by a number of researchers [2, 8] were used in this study. The ratios of the flexural capacities developed by the PT beam and the beam web FD are given in Table I. These ratios fall well within the ranges recommended by a number of researchers [2, 8]. The first digit (4 or 6) in the Specimen ID indicates the number of

DOI: 10.1002/eqe

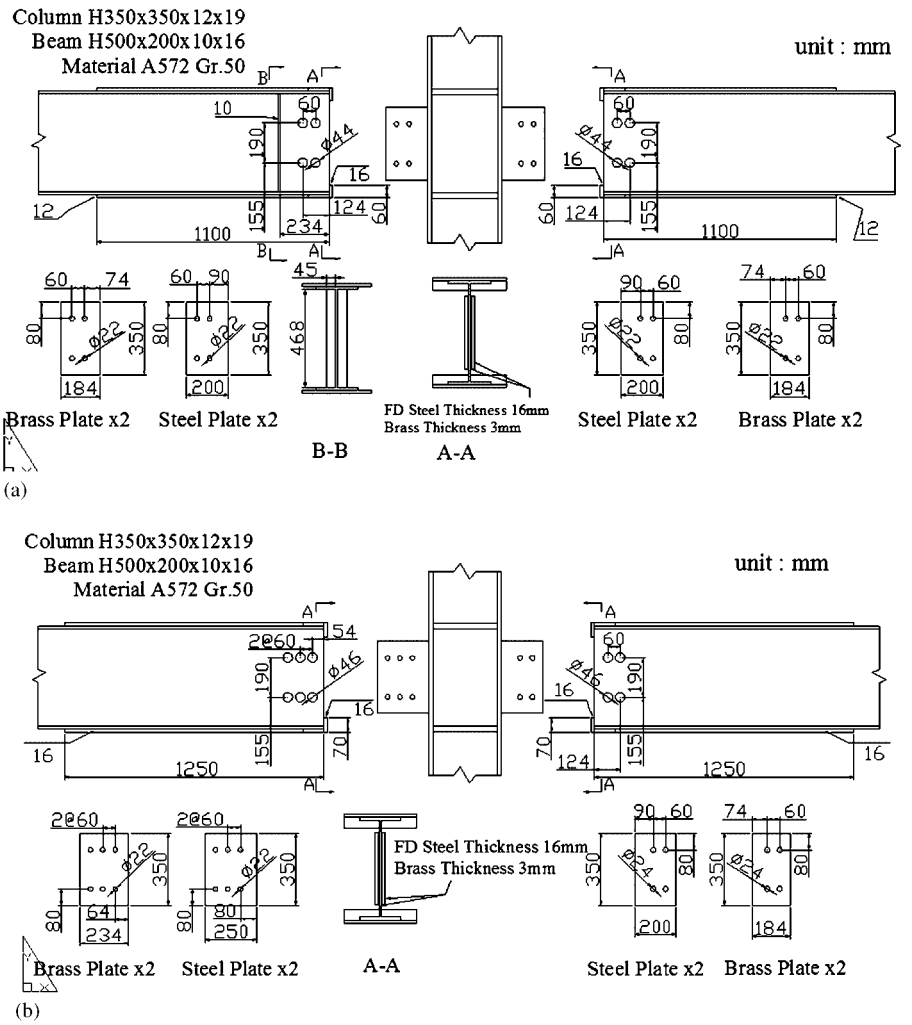

Figure 6. Details of PTFD connection specimens: (a) Specimens BWFD4B20 and BWFD4B20 and (b) Specimens BWFD6B22 and BWFD4F22.

bolts adopted in the FD. The second character (B or F) denotes the type of washers (Belleville or flat) used. The next two digits give the diameter (20 or 22 mm) of the F10 bolts. The character 'S' after the digit refers to the beam web stiffener. A friction coefficient of 0.34 is assumed in the design and analysis of all FDs. The analytical predictions for the four specimens are given in Figure 7. Key features of each specimen are described as follows.

4.1.1. Specimen BWFD 4B20S. The initial PT tendon force provided a flexural capacity $M_{\mathrm{pt},i}$ of about 40% of the beam nominal flexural capacity, M_p. Two tendons, each consisting of 5–15 mm diameter ASTM A416 GR270 strands, were pre-stressed to a total tension of 1280 kN. An FD

DOI: 10.1002/eqe

Table I. Schedule of specimens.

Specimen	$M_{\mathrm{pt},i}/M_p$	M_{f}/M_p	M_d/M_p	$M_{0.05}/M_p$	$F_{\mathrm{pt},i}/F_{\mathrm{pt},u}$	$F_{\mathrm{pt},0.05}/F_{\mathrm{pt},u}$	$F_{pt,I}$ (kN)
4B20S	0.4	0.15	0.55	0.68	0.49	0.64	1179
4B20	0.4	0.15	0.55	0.68	0.49	0.64	1140
6B20	0.4	0.24	0.64	0.77	0.49	0.64	1288
4F22	0.45	0.21	0.66	0.79	0.57	0.72	1439

Note: $M_{0.05}$ and $F_{\mathrm{pt},0.05}$ are the beam moment and tendon force when the beam-end rotation reaches 0.05 rad. $M_p = 750\,\mathrm{kN\,m}$, beam nominal flexural capacity.

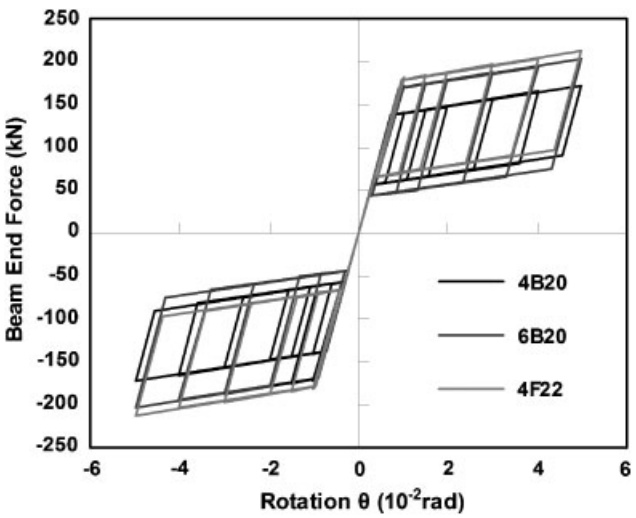

Figure 7. Analytical beam force *versus* rotation relationships.

flexural capacity M_{f} of $0.15M_p$ was considered in sizing the web bolted connection. Four 20 mm diameter F10T bolts together with four SHDS $45 \times 21 \times 5$-type Belleville washers were adopted in the FD. Two $350 \times 200 \times 16$ mm thick steel plates and two similar size but 3 mm thick brass plates were sandwiched over the beam web. The edges of the two outer steel plates were welded to the column flange. In order to prevent the web buckling near the FD, two 10 mm thick and 45 mm wide web stiffeners were welded to the beam web and flanges as shown in Figure 6(a).

4.1.2. Specimen BWFD 4B20. This specimen is identical to Specimen 4B20S but without any web stiffness.

4.1.3. Specimen BWFD 6B20. The initial PT tendon force provided a flexural capacity $M_{\mathrm{pt},i}$ of about $0.4M_p$, but a higher flexural capacity M_{f} of $0.24M_p$ was considered for the design of the FD. Six 20 mm diameter F10T bolts and six SHDS $45 \times 21 \times 5$-type Belleville washers were adopted, leading to the decompression moment of $0.64M_p$. Two $350 \times 250 \times 16$ mm thick steel plates and two similar in size but 3 mm thick brass plates were sandwiched over the beam web.

DOI: 10.1002/eqe

4.1.4. Specimen BWFD 4F22. The initial PT tendon force provided a slightly higher flexural capacity $M_{\mathrm{pt},i}$ of about $0.45M_p$. Two tendons, each consisting of 5–15 mm diameter ASTM A416 GR270 strands, were pre-stressed to a total tension of 1440 kN. An FD flexural capacity M_{f} of $0.21M_p$ was considered in sizing the web bolted connection. Four 22 mm diameter F10T bolts together with four flat washers were adopted in the FD. Two $350 \times 200 \times 16$ mm thick steel plates and two similar in size but 3 mm thick brass plates were sandwiched over the beam web.

4.2. Experimental responses of full-scale PTFD connections

The experimental setup is shown in Figure 8. Similar beam size with the same span was adopted in a companion study [4] to allow for convenient comparison of test results. Garlock [15] recommended that the PT system performance at various levels of earthquake should consider: (1) the entire system to remain elastic under a minor earthquake with a 50% probability of exceedance in 50 years; (2) the rotational demand of the PT beam-to-column connection be less than 0.035 rad for an earthquake with a 10% probability of exceedance in 50 years; (3) and less than 0.05 rad for an earthquake with a 2% probability of exceedance in 50 years. The cyclically increasing beam-end rotation protocol [6] as shown in Figure 9 was adopted. As noted above, each specimen was tested as a separate exterior beam-to-column connection. That is, when the left beam was tested, the right vertical actuator was detached from the beam. After all the single specimens were tested up to a peak rotation of 0.05 rad, Specimens 6B20 and 4F22 were tested simultaneously, just like for a typical interior beam-to-column connection subassembly, up to a peak rotation of 0.04 rad. The experimental responses of all the specimens are shown from Figures 10–14. The PT force was measured during each specimen test. No evidence of the anchor seating was found when the target drift was reached. Yielding of PT strands and buckling of the beam were also not observed in the tests. A reduction in the decompression moment has been found common in PT connections using various types of metallic energy dissipating devices [1, 2, 7], but the decompression moments in these PTFD connections remain essentially unchanged throughout the tests. The predictions made by using the equations presented in Section 2 are also plotted

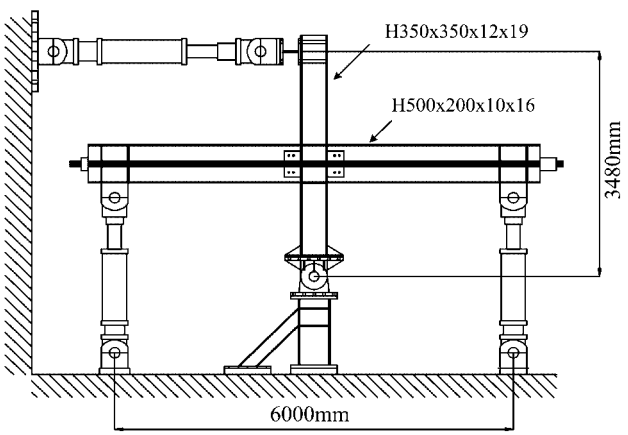

Figure 8. Experimental setup.

DOI: 10.1002/eqe

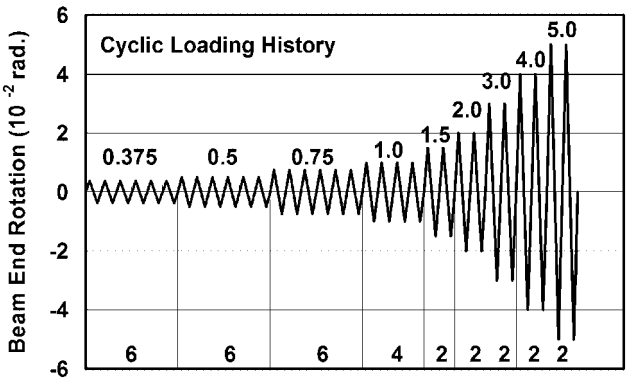

Figure 9. Standard cyclic loading protocol.

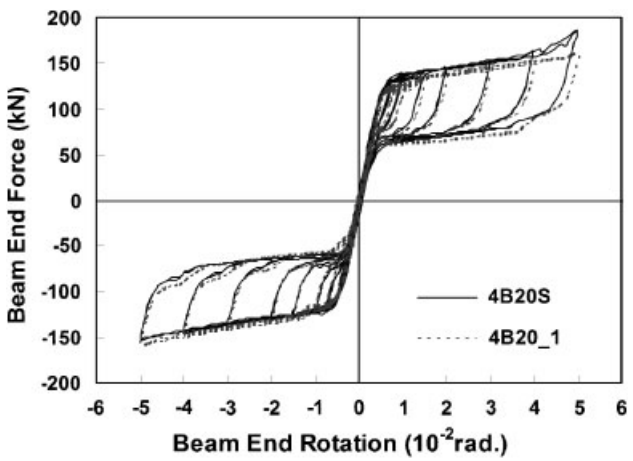

Figure 10. Experimental responses of Specimens 4B20S and 4B20.

from Figures 11–14. It is evident that the analytical responses agree well with the experimental results.

4.2.1. Specimens 4B20S and 4B20. Figure 10 shows that the experimental responses of Specimens 4B20S and 4B20 are very similar. It was noted that there was a sudden increase of the force responses in Specimen 4B20S when the beam-end deformation reached 0.05 rad. The beam was detached after the test, and it was found that there were bearing damages on the oversized bolt holes. Thus, the sudden increase of the post-yield stiffness noted above was due to the contact of bolt shank and the beam web at the edge of the oversized holes. In the erection of steel frames, the possibility of the holes being off-centered should be considered. The size of the oversized holes should be increased to accommodate the tolerance commonly prescribed for the construction practice. Figure 11 shows that the experimental responses are identical when Specimen 4B20 was

DOI: 10.1002/eqe

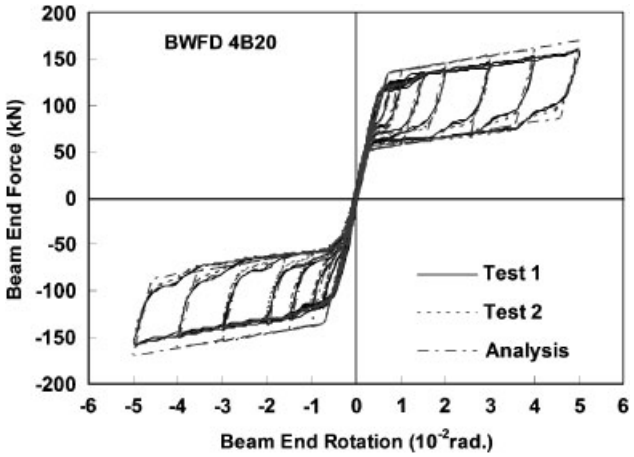

Figure 11. Test and analytical results of Specimen 4B20.

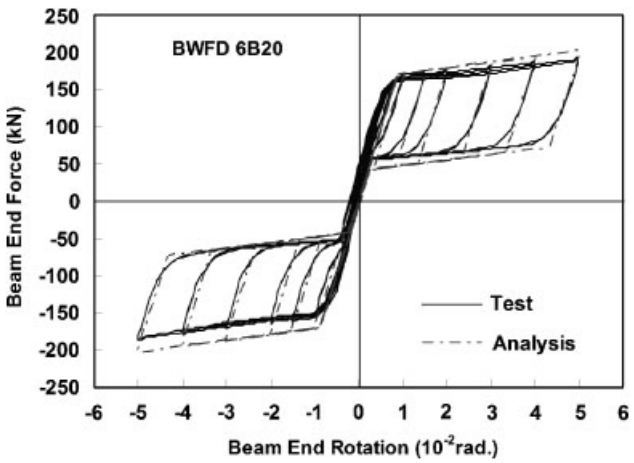

Figure 12. Test and analytical results of Specimen 6B20.

loaded twice with the AISC standard loading. The cyclic responses of Specimens 4B20S and 4B20 (Figures 10 and 11) show small kinks at the stiffness changes. However, this kind of kink was not observed in all other specimens; hence, it is suspected that there was a defect in the brass shim plates adopted in these specimens.

4.2.2. Specimens 6B20S and 4F22. Comparing the response of Specimen 6B20 (Figure 12) with that of Specimens 4B20S or 4B20 (Figure 10), it can be found that the area enclosed by the flag-shape hysteresis loops of Specimen 6B20 is larger due to higher friction force in the FD (see Table I). It is evident from Figure 13 that the experimental responses are identical when Specimen

DOI: 10.1002/eqe

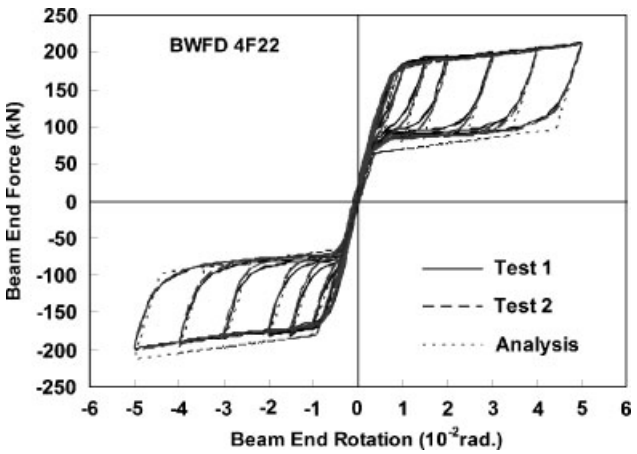

Figure 13. Test and analytical results of Specimen 4F22.

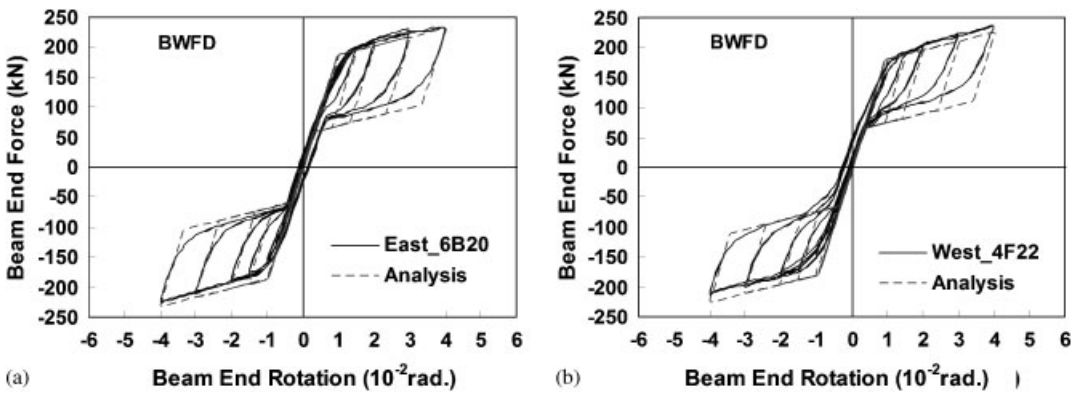

Figure 14. Experimental responses of Specimens 6B20 and 4F22 loaded simultaneously: (a) east beam and (b) west beam.

4F22 was subjected to twice the AISC standard loading. Comparing the responses of Specimen 6B20 (Figure 12) with that of Specimen 4F22 (Figure 13), it is found that the differences due to the effects of Belleville or flat washers are not pronounced. Comparing the responses of Specimen 4F22 (Figure 13) with those of other specimens (Figures 10 and 12), it can be found that Specimen 4F22 had the highest decompression moment (also see Table I).

After the single specimen tests, Specimens 6B20 and 4F22 were tested simultaneously up to a beam peak end rotation of 0.04 rad (Figure 14). Again, it is evident that the area enclosed by the hysteresis loops is larger in Specimen 6B20 than that in Specimen 4F22. In addition, Figure 14 shows that both beams had a greater post-yield stiffness than each had individually (see Figures 12 and 13). This is because when both beams were loaded simultaneously, the two beam-to-column gaps opened almost at the same time (Table I), leading to two times the tendon strain increment.

DOI: 10.1002/eqe

Figure 15. Specimens 6B20 and 4F22 after tests.

Table II. Experimental and analytical decompression moments at various beam-end rotations (kN m).

Rotation (%)	4B20S	4B20_1	4B20_2	6B20	4F22_1	4F22_2
0.75	350.8	339.3	325.4			
1	356.5	339.8	328.8	462.2	488.4	486.7
1.5	356.5	342.4	329.4	461.3	496.9	485.9
2	353.7	340.4	331.1	464.7	491.0	488.2
3	357.1	338.4	332.2	466.9	494.4	488.4
4	352.0	339.6	333.6	465.0	494.6	487.6
5	347.5	328.0	334.2	453.1	491.8	485.3
Analysis	391	381	381	480	507	507

Figure 15 shows the PT connection subassembly after the tests; no failure of the beam or column was observed.

4.3. Analysis of experimental results

4.3.1. Decompression moments. Table II gives the experimental and analytical decompression moments at each prescribed beam-end rotation. It is apparent that the experimental decompression moments remained about the same as the beam-end deformation increased. In general, the analyses over-estimated the experimental responses.

4.3.2. Effects of pre-tensions and FDs. It can be found from Table I that the magnitude of the clamping forces is controlled by the total number and size of the bolts. The contributions of the FDs on the flexural capacities of the PTFD connections range from 0.15 to 0.24. Figure 16 shows the experimental and analytical flexural contributions of the PT tendons and the FDs at various beam-end rotations. The experimental flexural contributions due to friction were computed by converting the bolt strain gauge readings into bolt tension first. The experimental friction force and bending

DOI: 10.1002/eqe

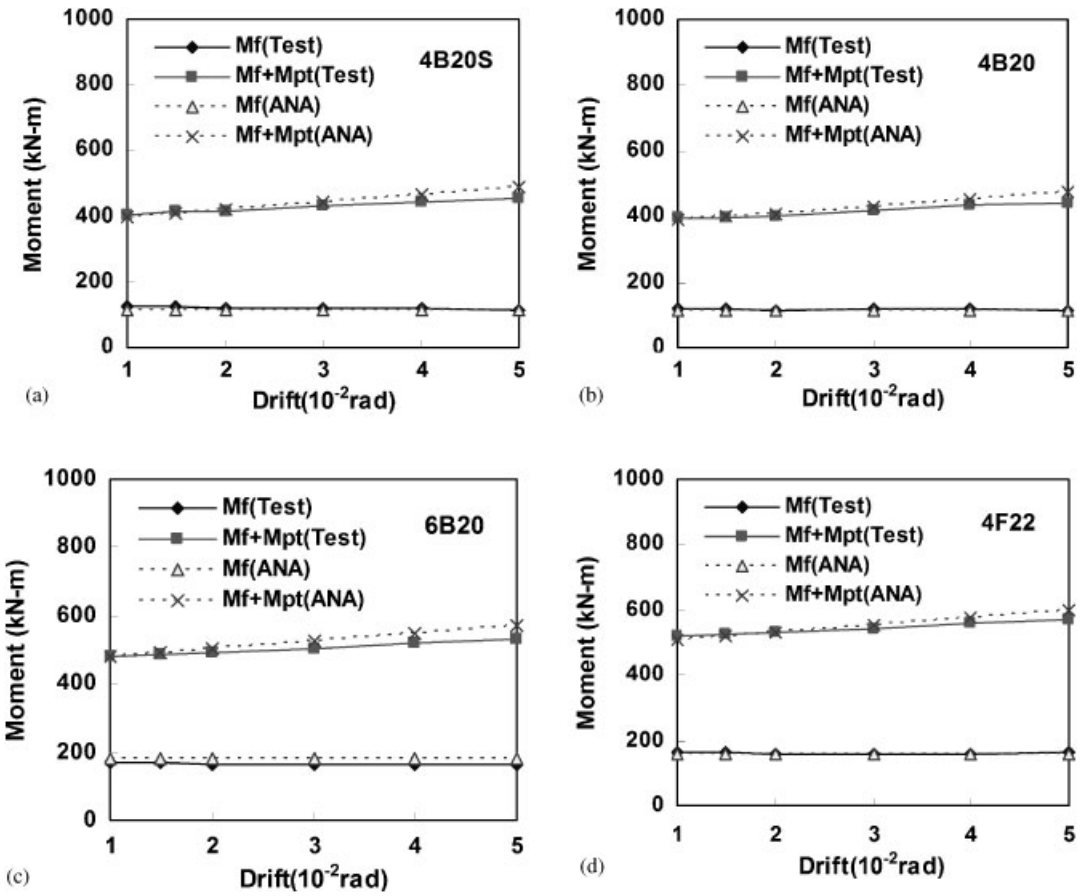

Figure 16. Experimental and analytical flexural contributions due to tendons and friction devices: (a) Specimen 4B20S; (b) Specimen 4B20; (c) Specimen 6B20; and (d) Specimen 4F22.

were then computed assuming a friction coefficient of 0.34. The flexural contributions due to the PT tendons were computed from the load cell readings. It is evident that the flexural contributions of the PT tendons and the FDs are predictable by comparing the test and analytical results. This seems to suggest that the flexural contribution of the FD can be computed by considering the total bolt clamping force and a friction coefficient of 0.34. This friction coefficient value of 0.34 was identified from the individual FD tests presented previously.

4.3.3. Energy dissipation capacity. From Figures 10–13 and 17, it can be found that the total hysteretic energy dissipated by the four connection specimens can be computed from the analytical model. The errors between the test and analytical results are about 3, 13, 9, and 4% for the four specimens, respectively. Low energy dissipation in these tests, when compared with a full self-centering system, is due to the number and size of the bolts adopted in the beam. If the beam depth is larger, more bolts could have been used to increase the energy dissipation.

DOI: 10.1002/eqe

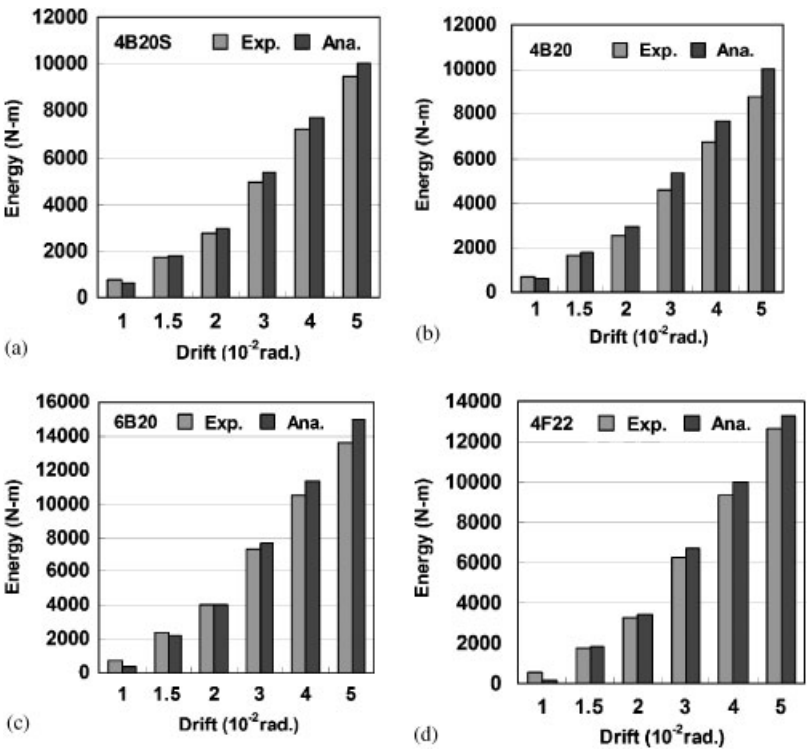

Figure 17. Experimental and analytical energy dissipations for each specimen: (a) Specimen 4B20S; (b) Specimen 4B20; (c) Specimen 6B20; and (d) Specimen 4F22.

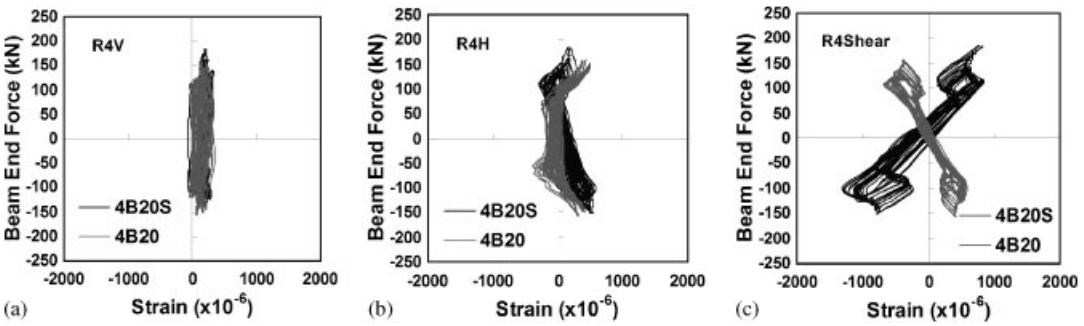

Figure 18. Strain gauge responses near the friction devices: (a) vertical strain readings; (b) horizontal strain readings; and (c) shear strain readings.

4.3.4. Effects of beam web stiffeners in specimen 4B20S. Strain gauges were placed near the FDs in Specimens 4B20S and 4B20. It is evident from Figure 18 that the strain readings in the rosettes were very similar. It suggests that the web stiffeners for Specimen 4B20S were not necessary.

DOI: 10.1002/eqe

5. CONCLUSIONS

Four PTED connections using BWFDs were designed and tested at NCREE to investigate cyclic performance. To determine the friction coefficient between brass and steel plates, four FD specimens were also tested. It is only found in the test of Specimen 4B20S that a sharp increase of the beam-end force was caused by the contact of bolts and the beam web at the edge of the oversized bolt holes. Therefore, it is recommended that a conservative approach should be taken in sizing the oversized bolt holes considering the construction tolerance requirements. Based on these tests and analyses, the following summary and conclusions are made:

(1) From the uni-axial tests of FDs, it is found that vibration and noise due to friction are more pronounced when the friction surface is new. In addition, friction forces tend to increase as cyclic displacements increase. When the friction surface has been worn before or when the Belleville washers are used, an almost constant friction force can be achieved. The friction coefficient between the steel plate and the brass shim is about the same for slotted or circular oversized hole patterns.
(2) Properly designed PTFD connections possess re-centering properties. The cyclic re-centering responses are identical when repeated cyclic loads are applied. The decompression moments also remain very much unchanged after many cycles of repeated large beam deformations. If the beams and the columns are designed to remain elastic, the proposed PTFD connections can sustain repeated large cyclic deformations without evidence of stiffness or strength degradation.
(3) The cyclic responses of the PTFD connections can be accurately predicted using the analytical methods outlined in this paper.

Note that if a PT frame is subjected to an excessive drift demand (i.e. larger than 5% drift), beam buckling similar to failures as expected in the welded moment-resisting frames might occur, leading to a loss of the re-centering property [4]. Furthermore, the restraining effects of the floor slab or the multiple columns on the opening of the gap at the beam-to-column interfaces could present challenges for the application of the proposed PT system. Therefore, these effects are being investigated in a joint effort of US–Taiwan researchers.

ACKNOWLEDGEMENTS

The National Science Council of Taiwan provided the financial support for this experimental research program. The laboratory supports provided by the NCREE are appreciated.

REFERENCES

1. Ricles JM, Sause R, Peng SW, Lu LW. Experimental evaluation of earthquake resistant posttensioned steel connections. *Journal of Structural Engineering* 2002; **128**(7):850–859.
2. Christopoulos C, Filiatrault A, Uang CM, Folz B. Posttensioned energy dissipating connections for moment-resisting steel frames. *Journal of Structural Engineering* 2002; **128**(9):1111–1120.
3. Garlock MM, Ricles MJ, Sause R. Experimental studies of full-scale posttensioned steel connections. *Journal of Structural Engineering* 2005; **131**(3):438–448.
4. Chou C-C, Chen J-H, Chen Y-C, Tsai K-C. Evaluating performance of post-tensioned steel connections with strands and reduced flange plates. *Earthquake Engineering and Structural Dynamics* 2006; **35**(9):1167–1185.

DOI: 10.1002/eqe

5. Chou C-C, Lai Y-J. Seismic resistant self-centering moment connections with bottom flange buckling-restrained energy dissipators. *Eighth Taiwan–Korea–Japan Joint Seminar on Earthquake Engineering for Building Structures*, Japan, 2006.
6. AISC. *Seismic Provisions for Structural Steel Buildings*. AISC: Chicago, IL, 2002.
7. Chou C-C, Yang W-C, Tsai K-C. Experimental evaluation of post-tensioned steel connections with steel bars and a discontinuous slab. *Seventh Japan–Taiwan–Korea Joint Seminar on Earthquake Engineering for Building Structures*, Korea, 2005.
8. Rojas P, Ricles MJ, Sause R. Seismic performance of post-tensioned steel moment resisting frames with friction devices. *Journal of Structural Engineering* 2005; **131**(4):529–540.
9. Wolski M, Ricles JM, Sause R, Lee KS. Energy dissipation for self-centering steel MRFs: bottom flange friction device. *US–Taiwan Workshop on Self-centering Structural System. NCREE-05-004*, Taipei, Taiwan, 2005; 16–18.
10. Tsai K-C, Chou C-C, Lin C-L. Seismic response of post-tensioned steel beam-to-column connections using friction devices. *NCREE Technical Report*, 2006 (in Chinese).
11. Englekirk R. *Steel Structures*. Wiley: New York, 1994.
12. Grigorian CE, Popov EP. Energy dissipation with slotted bolted connections. *Report No. UBC/EERC-94/02*, University of California, Berkeley, CA, 1994.
13. Morgen B, Kurama YC. A friction damper for post-tensioned precast concrete moment frames. *PCI Journal* 2004; **49**(4):112–132.
14. American Institute of Steel Construction, AISC. *Manual of Steel Construction*: *Load and Resistance Factor Design*. American Institute of Steel Construction: Chicago, IL, 2001.
15. Garlock M. Full-scale testing, seismic analysis, and design of post-tensioned seismic resistant connections for steel frames. *Ph.D. Dissertation*, Civil and Environmental Engineering Department, Lehigh University, Bethlehem, PA, 2002.

DOI: 10.1002/eqe